Management of three-dimensional intrafraction motion through real-time DMLC tracking

Amit Sawant,[a] Raghu Venkat, Vikram Srivastava, and David Carlson
Department of Radiation Oncology, Stanford University, Stanford, California 94305

Sergey Povzner and Herb Cattell
Varian Medical Systems, Palo Alto, California 94304

Paul Keall
Department of Radiation Oncology, Stanford University, Stanford, California 94305

(Received 18 September 2007; revised 18 February 2008; accepted for publication 15 March 2008; published 25 April 2008)

Tumor tracking using a dynamic multileaf collimator (DMLC) represents a promising approach for intrafraction motion management in thoracic and abdominal cancer radiotherapy. In this work, we develop, empirically demonstrate, and characterize a novel 3D tracking algorithm for real-time, conformal, intensity modulated radiotherapy (IMRT) and volumetric modulated arc therapy (VMAT)-based radiation delivery to targets moving in three dimensions. The algorithm obtains real-time information of target location from an independent position monitoring system and dynamically calculates MLC leaf positions to account for changes in target position. Initial studies were performed to evaluate the geometric accuracy of DMLC tracking of 3D target motion. In addition, dosimetric studies were performed on a clinical linac to evaluate the impact of real-time DMLC tracking for conformal, step-and-shoot (S-IMRT), dynamic (D-IMRT), and VMAT deliveries to a moving target. The efficiency of conformal and IMRT delivery in the presence of tracking was determined. Results show that submillimeter geometric accuracy in all three dimensions is achievable with DMLC tracking. Significant dosimetric improvements were observed in the presence of tracking for conformal and IMRT deliveries to moving targets. A gamma index evaluation with a 3%–3 mm criterion showed that deliveries without DMLC tracking exhibit between 1.7 (S-IMRT) and 4.8 (D-IMRT) times more dose points that fail the evaluation compared to corresponding deliveries with tracking. The efficiency of IMRT delivery, as measured in the lab, was observed to be significantly lower in case of tracking target motion perpendicular to MLC leaf travel compared to motion parallel to leaf travel. Nevertheless, these early results indicate that accurate, real-time DMLC tracking of 3D tumor motion is feasible and can potentially result in significant geometric and dosimetric advantages leading to more effective management of intrafraction motion. © *2008 American Association of Physicists in Medicine*. [DOI: 10.1118/1.2905355]

Key words: IGRT, adaptive radiotherapy, real-time, tumor tracking, dynamic MLC, intrafraction motion

I. INTRODUCTION

Intrafraction motion results in significant geometric and dosimetric uncertainties in radiation treatment planning and dose delivery.[1–3] Recently, much attention has been given to the effective management of such motion, particularly, in the context of treating thoracic and abdominal tumors.[4] This increased interest can be attributed to several factors, among which the following are particularly noteworthy. First, a number of recent clinical studies have systematically quantified the benefits of dose escalation to the tumor target region.[5–7] as well as the probability of increased complications arising from excessive irradiation of surrounding normal tissue and critical structures.[8,9] Such studies have underscored the "intuitively recognized" need for achieving greater geometric precision in treatment planning and delivery. Concurrently, rapid progress in pretreatment imaging (e.g., high-resolution, multislice 4DCT), sophisticated computerized treatment planning, and the development of delivery techniques such as intensity modulated radiotherapy (IMRT) and volumetric modulated arc therapy (VMAT) have given us the capability of precisely delineating and irradiating the tumor target. As a result, the goal of routinely achieving submillimeter targeting accuracy during dose delivery is coming ever closer to clinical reality.

The problem of intrafraction motion management can be viewed to consist of two distinct and, in principle, independent tasks: (i) real-time estimation of target position and (ii) real-time repositioning/modulation of the treatment beam relative to the estimated target position. Techniques to estimate target position are based on imaging external markers, implanted (internal) markers, or internal anatomic structures.[10–17] Information obtained from one or more of these techniques serves as input for the next task—i.e., real-time beam repositioning. This task can be accomplished using a variety of motion-compensation strategies such as moving the x-ray source,[18–20] moving the treatment couch,[21]

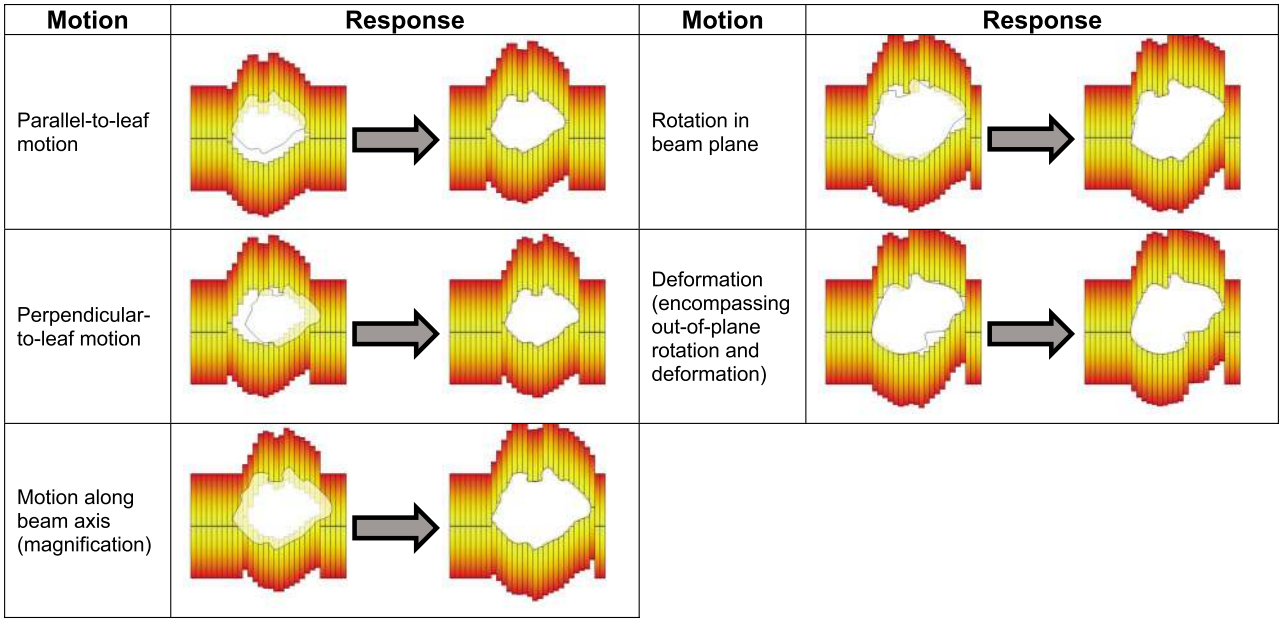

FIG. 1. Schematic illustration of the various types of target motion as seen in the beam's view and the desired change in MLC configuration to account for each type of motion.

or gating the radiation beam within a specified time/phase window.[22–28] Other approaches to intrafraction motion management are breath hold[29–31] and abdominal compression,[32,33] but are not considered further in this article.

One promising approach for beam repositioning is the use of a dynamic multileaf collimator (DMLC) to continuously align and/or reshape the treatment aperture(s) so as to compensate for target motion. (We refer to this process as DMLC tracking). Theoretical investigations of DMLC-based IMRT have been reported for deforming targets moving in one dimension (1D)[34,35] and two dimensions (2D).[36,37] DMLC tracking of 1D, rigid-body motion has been empirically demonstrated and characterized by our group.[38] The results obtained from these theoretical and empirical studies suggest that there exists significant potential for improved dosimetric accuracy with the use of real-time tracking. Furthermore, these dosimetric advantages are expected to improve as tracking techniques account for progressively more complex target motion.

In this work, we develop, demonstrate and characterize a robust DMLC tracking algorithm that obtains real-time information of target location from an independent position monitoring system, and dynamically repositions the beam to account for 3D target motion. It should be noted that in the context of the present work, the term real-time is used to denote a time duration that is much less than the time scale of the motion being studied. Furthermore, the beam repositioning and/or modulation described in this work indicate a dynamic change in the delivered fluence through modifying the geometric shape of the beam aperture. It is indeed possible to envisage more sophisticated forms of 4D adaptation, involving real-time reoptimization of the treatment plan and/or real-time variation of the dose rate (a feature unavailable on current linacs). However, such strategies are beyond the scope of the present work.

Early empirical studies of geometric and dosimetric tracking accuracy are presented. These studies include conformal and IMRT delivery to a moving phantom, using a laboratory DMLC-based tracking system as well as a clinical linac.

II. TARGET MOTION AND DMLC TRACKING

The overall objective of DMLC tracking is to dynamically reposition each MLC leaf so as to achieve the delivery of a desired fluence to a target that is continuously changing its spatial location and/or shape in the beam's view. As illustrated in Fig. 1, target motion in the beam's view may be classified into the following types:

(1) Rigid translation in the treatment plane (i.e., the isocentric plane perpendicular to the beam axis), including motion both parallel and perpendicular to MLC leaf travel direction.
(2) Rigid translation along the beam direction, resulting in magnification/demagnification in the treatment plane.
(3) Rigid in-plane rotation.
(4) Rigid out-of-plane rotation and deformation (both of which result in a change in the target shape in the beam's view).

Also shown is the desired repositioning of the MLC leaves for each type of motion.

Previous work has shown that real-time information of the aforementioned forms of target motion can be obtained using external and/or internal surrogates.[10–17] The tracking algorithm developed in this work uses such information and dy-

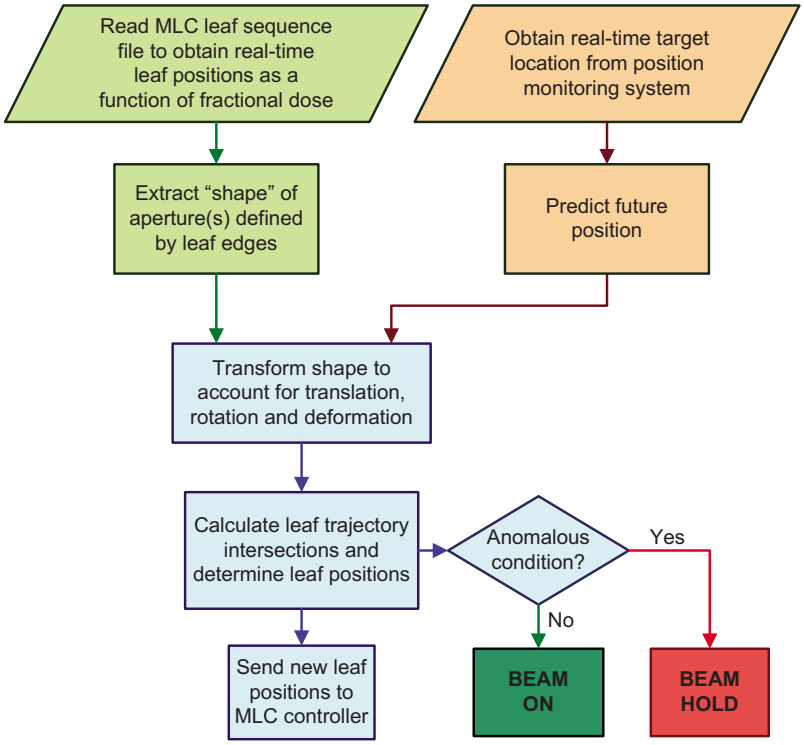

FIG. 2. Logical flow of the real-time DMLC tracking algorithm.

namically recalculates the position of each MLC leaf so as to best account for target motion. It should be noted that, in its current implementation, the algorithm accounts for 3D rigid translation (Fig. 1, steps 1–3). However, the formalism developed here is extendable to include more complex types of motion (Fig. 1, steps 4 and 5).

III. METHODS

III.A. DMLC tracking algorithm

The following general design principles have been used in the development of the MLC tracking methodology:

(i) At every time point, the MLC leaves are positioned so as to best approximate the instantaneous geometric shape of the aperture(s).
(ii) Integral fluence at the target plane is conserved at all times.
(iii) Radiation through the tips of closed MLC leaves is minimized by moving "nontracking" leaf pairs under the nearest jaw.
(iv) The beam is turned off in anomalous situations and the leaves continue to track target motion.

It should be noted that, in order to truly achieve the goal outlined in (2), the linac would be required to dynamically change monitor units (MUs) based on (a) inverse square and tissue maximum ratio corrections so as to compensate for motion along the beam direction and (b) change in off-axis ratios to account for motion perpendicular to the beam axis.[39] Such real-time change in MUs is not currently possible on our laboratory system or existing clinical systems and is therefore not further considered in the present study.

Figure 2 shows the overall logical flow of the DMLC tracking algorithm. The key elements in this algorithm are described next.

(1) **Initial leaf positions**: The leaf sequence file derived from the treatment plan contains MLC leaf positions defined as a function of MU. At each "control point" defined in the file, the MLC leaves form one or more beam apertures so as to deliver a desired fluence. The tracking algorithm reads in these leaf positions (linearly interpolating between control points based on delivered MU) and extracts the shape defined by the leaf edges (Fig. 3). This shape may be represented as $L(MU,x,y)$, where (x,y) are the 2D spatial coordinates of each leaf corner, as projected on the treatment plane. (For an MLC with N leaves, the shape will comprise of 2N points.)
(2) **Target motion**: In the present implementation of the algorithm, the instantaneous target position in 3D is estimated using an independent real-time position monitoring system (RPM, ver 1.7, Varian Medical Systems, Palo Alto, CA). It is important to note that this information represents a best estimate of the actual target position based on the correlation established between the marker block and the target centroid from the planning CT images.

The 3D translational motion recorded by the position

monitoring system is reported in the room coordinate system. Due to the fact that most modern delivery techniques irradiate the patient from multiple angular orientations of gantry, collimator and couch, the 3D translational motion vector (x,y,z) is transformed from the room coordinates to a coordinate system corresponding to the beam's eye view. This transformation is performed via a rotation matrix to yield

$$\begin{pmatrix} x' \\ y' \\ z' \end{pmatrix} = \begin{pmatrix} x[\cos\alpha\sin\beta\cos\gamma+\cos\beta\sin\gamma]+y[\sin\alpha\sin\beta]+z[\cos\alpha\sin\beta\sin\gamma-\cos\beta\cos\gamma] \\ x[\sin\alpha\cos\gamma]+y[-\cos\alpha]+z[\sin\alpha\sin\gamma] \\ x[-\cos\alpha\cos\beta\cos\gamma+\sin\beta\sin\gamma]+y[-\sin\alpha\cos\beta]+z[-\cos\alpha\cos\beta\sin\gamma-\sin\beta\cos\gamma] \end{pmatrix}, \quad (1)$$

where (x',y',z') is the transformed vector in the beam's eye view and α, β, and γ are the rotation angles of the gantry, collimator and couch, respectively, in the room coordinate system.

(3) **Prediction**: There exists an inherent temporal latency associated with the processes of detecting target motion, calculating new positions by the tracking algorithm, and the response time of the MLC leaves. In order to compensate for such latency, the position of the target at time T(t+Δ) is predicted, where Δ represents the amount of temporal latency (measured to be ~160 ms for our lab system).[40] In the present implementation, the algorithm uses a modified linear adaptive filter with a user-defined prediction window to estimate future position.[41]

(4) **Transform MLC shape to account for target motion**: The information about target motion in the beam's eye view obtained from Eq. (1) is used to remap each point of the original MLC shape $L(MU,X,Y)$ to a new location (X',Y') on the treatment plane. This process can be represented as

$$L(MU,X,Y) \overset{R(X,Y)}{\Rightarrow} L^R(MU,X',Y'), \quad (2)$$

where $R(X,Y)$ is termed as the relocation vector. For rigid body motion, $R(X,Y)$ is constant for the entire shape and is derived from

$$R(X,Y) \equiv (x'+\Delta x_{z'}, y'+\Delta y_{z'}), \quad (3)$$

where $\Delta x_{z'}$ and $\Delta y_{Z'}$ are the x and y projections, respectively, of displacement along the beam axis (z) onto the treatment plane. Since this is a purely geometric remapping that ignores higher order effects such as off-axis corrections, dose inhomogeneities, etc., the nature of the process that causes the 3D displacement (translation, rotation, or deformation of the target) is transparent to this calculation. Similar geometric, aperture-transformation strategies, based on CT-image guidance have been proposed elsewhere to account for interfraction motion.[42,43]

(5) **Calculate new leaf positions**: The next step is to find the best fit of the MLC leaves to this new shape. The relocated points are sequentially joined to form line segments. In its simplest implementation, leaf fitting is performed by determining the points of intersection of each leaf-pair trajectory with the segments constituting the aperture(s), as shown in Fig. 3. Each leaf position is recalculated so that the midpoint of the leaf outer edge goes to the nearest point of intersection. While this method is simple to implement, the precision of leaf fitting is limited due to finite leaf width. The potential error that may occur as a result of such discretization is illustrated in Fig. 4(a). Moreover, multiple applications of this technique may result in systematic expansion or contraction of an aperture.

Obviously, a "perfect fit" to an arbitrary shape cannot be achieved using leaves of finite width—a problem common to all MLC-based conformal radiotherapy. One strategy to minimize the geometric and thereby, dosimetric error is to position the leaves so that the overdosed and the underdosed regions in the treatment plane are approximately equal. (The overdosed region is the area that is outside the calculated shape but open to the beam, while the underdosed region is the area within the shape but under the leaves.) In the present work, this objective is achieved by dividing each leaf into virtual "subleaves" [Fig. 4(b)]. The intersections of each subtrajectory with the segments of the shape are determined. The point of intersection of the parent leaf is then calculated as the average of the corresponding subtrajectory intersections. A similar technique has recently been described by McClelland *et al.*.[36]

(6) **Minimize radiation leakage through leaf tips**: There occurs a small but significant amount of radiation leakage through the tips of closed MLC leaves.[44,45] As shown in Fig. 3, the algorithm attempts to minimize such leakage radiation by moving the MLC leaf pairs that do not participate in the tracking process under the nearest jaws. In the process of tracking target motion perpendicular to the direction of leaf travel, leaves that are positioned at the periphery of an aperture at a given time instant may need to become part of the aperture in the next time instant. In order to ensure that a leaf pair does not have to move suddenly from beneath the jaws to form an aperture, some leaf pairs on either side of the original aperture are positioned at the center of the leaf opening for the leaf pairs, defining the extent of the ap-

1	Read initial leaf positions from MLC file.	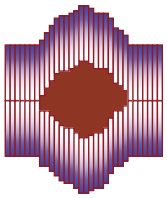
2	Extract the "shape" defined by the points corresponding to MLC leaf tips.	
3	Transform this shape to match real-time target position/shape (estimated from a real-time position monitoring system).	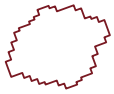
4	Determine the intersection points of MLC leaf trajectories with the transformed shape.	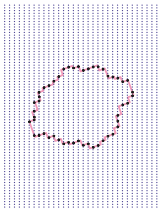
5	Send MLC leaves to the points of intersection. Closed leaf pairs adjacent to open aperture(s) are positioned at the midpoint of nearest open leaf pair. Peripheral closed leaf pairs are sent beneath the nearest jaw.	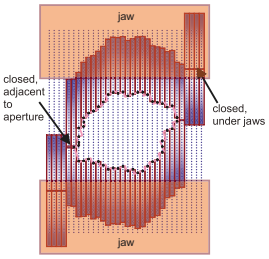

FIG. 3. Schematic illustration of the key steps in the tracking algorithm.

erture and abut to its opposing leaf (Fig. 3). The number of adjacent closed leaf pairs is estimated from the extent of target motion in the perpendicular direction. Note that if there are multiple open apertures on either side of an adjacent leaf pair, then these (closed) leaves are directed to the nearest open leaf pair on either side. Sending and retrieving leaf pairs from under the jaws to the adjacent state is performed using a velocity of 3.0 cm s^{-1} (below the maximum velocity for this MLC type[40]) to ensure this process does not contribute to a beam hold.

(7) **Anomalous conditions**: While most intrafraction motion can be considered to be somewhat predictable in terms of magnitude and/or frequency, a variety of situations may occur that require the dose delivery to be paused. For example, the position monitoring system may detect irregular motion due to large shifts in patient position during treatment, a sudden change in respiratory pattern, bowel movement, swallowing, coughing, etc. In some cases, the motion may be faster than the MLC leaves can track or the motion may necessitate one or more MLC leaves to move beyond their travel range (14.5 cm in the case of our system). The aperture may move beneath the primary jaws. Each of these cases is potentially representative of an undesirable situation where the patient may be hyperventilating, breathing too erratically, or the position monitoring marker may have fallen off or been displaced. In all such cases, rather than treat with big uncertainties, the algorithm makes the conservative choice of pausing the beam while the anomalous condition persists. At the same time, the DMLC leaves continue to track target motion so that dose delivery can be resumed as soon as the anomalous condition stops, thus maximizing delivery efficiency. Note that turning the beam off and on in response to anomalous conditions impacts only the delivery efficiency and has no impact on the dosimetric accuracy.

III.B. Experimental studies

Preliminary studies were performed in order to empirically demonstrate the DMLC tracking algorithm and characterize it in terms of geometric and dosimetric accuracy and

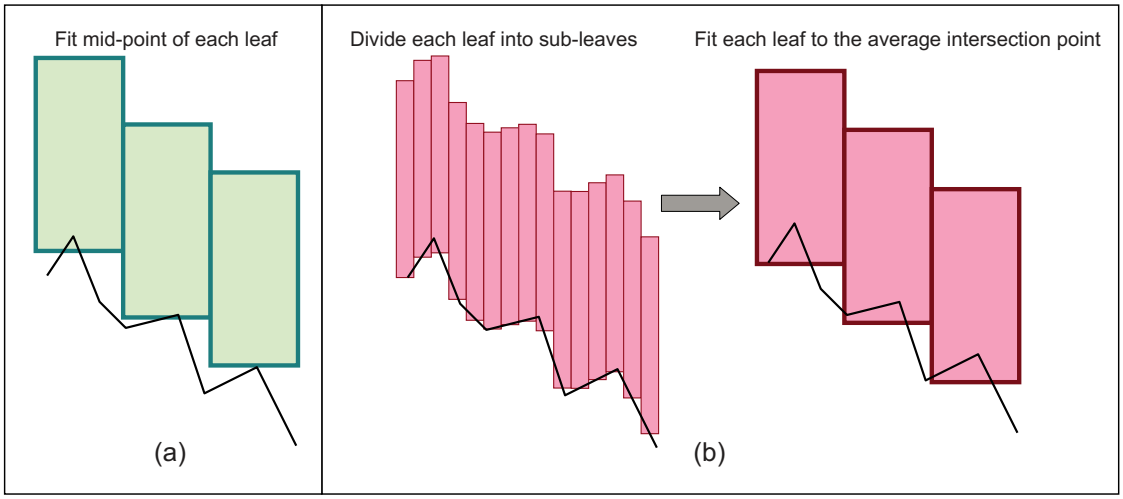

FIG. 4. Schematic illustration of the leaf fitting operation (a) without and (b) with the use of subleaves.

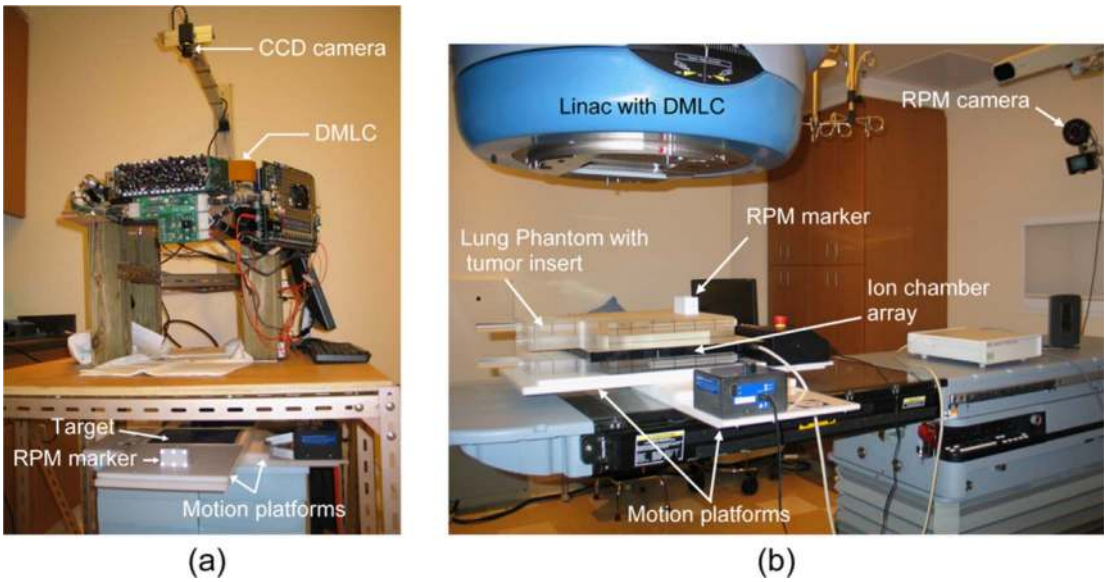

FIG. 5. Experimental arrangement for tracking studies using (a) the lab system and (b) a clinical system.

delivery efficiency. While the algorithm can also be used for tracking relatively slow and aperiodic motion (e.g., prostate motion), in the present work, the more challenging task of tracking respiratory motion was considered.

Two-dimensional in-plane rigid-body motion was simulated by placing a "target" on two orthogonally oriented linear motion platforms (Fig. 5), each programmed with a sinusoidal motion pattern. The platforms were aligned so as to move parallel (20 mm) and perpendicular (5 mm) to the direction of MLC leaf motion. In addition, the motion of the two platforms was deliberately set out of phase, thus tracing an elliptical path so as to simulate hysteresis, which is commonly observed in lung tumor motion.[46] Due to limitations of our present setup, motion along the beam axis was simulated only for geometric studies (performed in the lab) using a separate motion platform (not shown for brevity) that was programmed to move sinusoidally, 25 mm along the beam axis. Note that the range of travel in each direction was chosen so as to encompass the vast majority of observed respiratory motion.[4,46–48] Finally, unless otherwise noted, all measurements were performed using five virtual subleaves (Sec. III A 5) per MLC leaf.

III.B.1. Geometric accuracy

A previously designed laboratory DMLC tracking system[38] was used to demonstrate and characterize the geometric tracking accuracy of the algorithm. The experimental arrangement is described in detail elsewhere[38] and is briefly summarized as follows. The setup [Fig. 5(a)] involved a DMLC (Millennium, 120-leaf, Varian Medical Systems, Palo Alto, CA) and the RPM (ver 1.7) system. The MLC leaves were programmed to form a circular aperture. The two orthogonally oriented linear motion platforms were positioned under the MLC and a grid pattern with 20 mm × 20 mm squares [Fig. 6(a)] was placed on the upper platform along with the RPM marker block, which was comprised of six infrared, reflective markers. A separate motion platform (in conjunction with the RPM block) and a different pattern, consisting of a white circle against a dark background [Fig. 6(b)], were used to quantify tracking accuracy along the beam axis.

The RPM system acquired sequential images of the marker block at 30 Hz in order to estimate its real-time 3D position, which was communicated to the tracking computer via serial port. This information was used by the tracking algorithm to calculate new leaf positions, which were sent via Ethernet to an MLC controller, which in turn actuated the mechanical movement of the MLC leaves. Real-time beam's-eye-view videos of the in-plane and the vertical

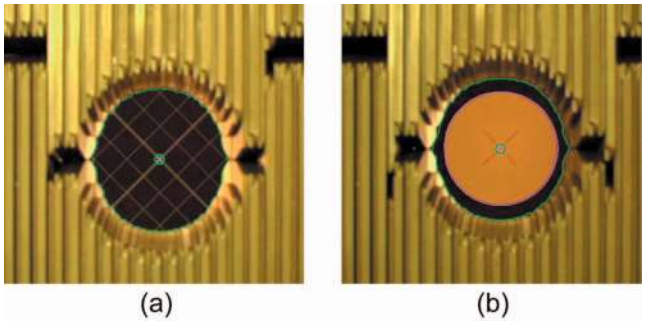

FIG. 6. Image frames extracted from tracking movies acquired to determine the geometric accuracy of DMLC tracking. Two different patterns were separately mounted on the motion platforms to calculate tracking accuracy of (a) motion parallel and perpendicular to MLC leaf travel and (b) motion along the beam axis. In each case, the image frames were segmented in order to determine the peripheral bounds and the center of the MLC aperture (indicated by the outer and inner green circles, respectively) and the central point on the underlying geometric pattern (indicated by the magenta cross). The image frames of the geometric pattern used in (b) were also segmented to delineate the boundary of the white circle (indicated by the magenta outline).

tracking processes were acquired using an independent 640×480 format color CCD camera (Toshiba Teli, Concord, CA) operating at 15 Hz.

In the case of 2D in-plane target motion, individual image frames were extracted from the video and segmented in order to determine the locations of the centroid of the circular MLC aperture and the crosshairs of the grid pattern [Fig. 6(a)]. The dimensions of the squares of the grid pattern ($20\ \text{mm} \times 20\ \text{mm}$) were used to determine the relationship between the image pixels in each frame and the absolute distance in millimeters. Geometric tracking error was calculated in each frame from the absolute positional difference between the aperture centroid and the target crosshairs. In order to visually illustrate the algorithm, a movie of MLC tracking for a conformal field has been added to the submission as EPAPS.[56]

Tracking accuracy along the beam axis was determined as follows. In this case, the image frames extracted from the tracking video were segmented to determine the inner and outer boundaries of the MLC aperture and the white circle, respectively. The radii of the MLC aperture and the circle were calculated in each segmented frame from the areas within their respective boundaries. Ideally, the radius of the aperture should change in exact proportion to that of the circle as the latter undergoes magnification/demagnification in the beam's view. Deviation from this behavior implies geometric error in the tracking process. Due to the fact that the inner circle was necessarily smaller than the MLC aperture (so as to facilitate segmentation), the two radii were normalized by applying a multiplicative scaling factor to the radius of the circle in each image frame. The scaling factor was calculated from the ratio of the mean radius of the aperture to the mean radius of the circle across all image frames. (Consequently, the mean values of the two radii were equal.) The geometric tracking error in each image frame was then calculated as the absolute difference between the radius of the MLC aperture and the scaled radius of the circle.

III.B.2. Delivery efficiency

Real-time DMLC tracking has the potential to achieve 100% efficiency due to the fact that the MLC attempts to cover the target at all times throughout the delivery. However, in practice, delivery efficiency is limited by a combination of several factors, such as the complexity of the leaf sequence, target velocity and the maximum possible leaf velocity, and acceleration of the MLC system. Delivery efficiency was determined in the lab by simulating a dose delivery of 100 MU at 300 MU/min for a conformal (circular) field and clinically-derived step-and-shoot (S-IMRT) and dynamic (D-IMRT) deliveries. Efficiency was calculated from the ratio of the times required to complete the programmed delivery in the absence and presence of motion tracking. The measurements were obtained independently in the parallel (20 mm amplitude) and perpendicular (5 mm amplitude) directions by progressively increasing the frequency of motion of the corresponding linear motion table.

III.B.3. Dosimetric studies

DMLC tracking of 2D rigid-body motion was performed on a clinical system in order to study potential dosimetric differences in the presence and absence of tracking. The experimental arrangement is shown in Fig. 5(b). A lung phantom was irradiated using a clinical linac (Trilogy, Varian Medical Systems, Palo Alto, CA) equipped with a DMLC and the RPM system. The linac was operated in service mode and the output of the RPM system was rerouted to our in-house DMLC tracking computer. New leaf positions calculated by the tracking algorithm were sent via Ethernet to the MLC controller of the linac. The phantom (comprised of four acrylic slabs, each 5 cm thick) had a lung tissue-equivalent insert, which in turn contained an embedded tumor-equivalent object. The lung insert was sandwiched between 10 cm of acrylic on each side. The phantom was oriented such that the "tumor" was positioned at the isocenter. A 2D ionization chamber array comprising a matrix of 27×27 ionization chambers (PTW-seven29, Freiburg, Germany) was placed immediately below the tumor insert to obtain dose measurements. The entire assembly was mounted on the two orthogonally-oriented linear motion platforms moving in a sinusoidal pattern at 0.25 Hz, in order to simulate elliptical motion (as described in Sec. II B). In this arrangement, the dosimeter array moved in conjunction with the tumor at all times. Dosimetric measurements were obtained for 100 MU delivered at 300 MU/s, for the same circular and the D-IMRT fields that were used in the laboratory measurements. A clinically-derived S-IMRT was also performed for the same dose. In addition, a VMAT delivery of 300 MU at a dose rate of 300 MU/min was also performed. The delivery was performed for a 290° arc with collimator and couch angles of 45° and 180°, respectively. Further details of the VMAT technique may be found elsewhere.[49]

For each of the delivery techniques the following measurements were obtained—(1) static target and dose delivery without MLC tracking, (2) moving target and delivery without MLC tracking, and (3) moving target with MLC tracking. The dosimetric impact of DMLC tracking was quantified via a gamma index evaluation that compared the dose distributions obtained for delivery to a moving target in the absence and presence of tracking to the corresponding delivery to a static target. The gamma index was calculated using a stand-alone software (PTW-Verisoft 3.0) with a 3% dose—3 mm criterion. In each case, the number of dose points receiving within 3% of the maximum dose on the reference (i.e., corresponding delivery to a static target) and failing the gamma metric was determined.

IV. RESULTS

Image frames extracted from the tracking video are shown in Fig. 6. The adjacent closed leaf pairs (see Sec. III A 6) can be seen clearly on either side of the circular aperture. The tips of other closed leaf pairs can be observed near the top of the image, corresponding to a position under the linac jaws. Note that for the laboratory system (not the clinical system),

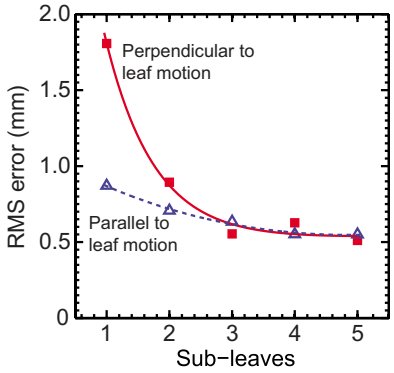

FIG. 7. Geometric tracking error in the parallel and perpendicular directions as a function of the number of virtual subleaves used in the DMLC tracking algorithm.

due to service access and mounting issues, the MLC is upside down with respect to the source and target.

The impact of using the subleaf concept can be observed in Fig. 7, which shows the root-mean-square (RMS) geometric error in the directions parallel and perpendicular to leaf motion as a function of the number of subleaves. In the perpendicular direction, the RMS error reduces rapidly as the number of subleaves increases beyond two. In contrast, for the parallel direction, where the step-size of each leaf is already quite small (~0.05 mm), oversampling of leaf trajectories appears to have a relatively smaller impact on accuracy. Finally, for both parallel and perpendicular directions, accuracy improves minimally beyond three subleaves, indicating a point of diminishing returns. Therefore, as a conservative choice, the number of subleaves was chosen to be five for all subsequent studies in the present work.

The geometric tracking error in the parallel [Fig. 8(a)], perpendicular [Fig. 8(b)], and the in-beam-line [Fig. 8(c)] directions is shown. While the use of virtual subleaves of leaf trajectories does reduce tracking error in the perpendicular direction, the ultimate resolution in this direction is nevertheless limited by finite leaf width. Consequently, the relative error (i.e., compared to the range of motion) in the perpendicular direction is significantly higher (~10%) than that observed in the parallel direction (~3%).

As expected, the relative tracking error for motion along the beam axis (~7%) lies between the values observed in the cases of tracking along parallel and perpendicular directions. It is also observed that a motion of ~25 mm along the beam axis results in relatively small positional changes (~2 mm) in the treatment plane due to target magnification/demagnification. Finally, it is important to note that in all three cases, the geometric error is significantly below one millimeter, indicating that submillimeter targeting accuracy in three dimensions is achievable using DMLC tracking.

Figure 9 shows the efficiency for conformal, D-IMRT, and S-IMRT deliveries as a function of frequency of motion, which is proportional to target velocity. Efficiency results are not shown for the VMAT delivery because for this technique the manufacturer's MLC controller software specifies larger leaf tolerances (~1 cm compared to 0.5 cm for IMRT) in order to avoid sudden stopping of the gantry due to a controller-asserted beam hold. As a result, the "efficiency" of VMAT delivery in the present implementation was 100% across the frequency range. For the conformal and IMRT deliveries, in each case the efficiency drops with increasing frequency. It should be noted that the absolute values shown in the figures are representative of the lab MLC system and correspond to the specific plans delivered rather than an average of many plans. Nevertheless, a relative comparison of these results provides a number of valuable insights.

In the case of conformal delivery, the drop in efficiency is sharper in the parallel direction [Fig. 9(a)] compared to the perpendicular direction [Fig. 9(b)]. Due to the fact that the shape of the conformal field used in the present study was a circle, the distance that each leaf had to travel in order to track perpendicular motion was relatively small. Even at the highest frequency, this distance was reasonably within the maximum leaf-velocity limit (~3.5 cm/s).[40] In the parallel direction, each leaf was required to track the entire motion (20 mm) and as the frequency increased, some leaves could not reach their desired positions. In such instances, the MLC controller asserted a beam-hold, thereby reducing the delivery efficiency.

In contrast, the D-IMRT and S-IMRT results show a significantly sharper falloff in efficiency in the perpendicular

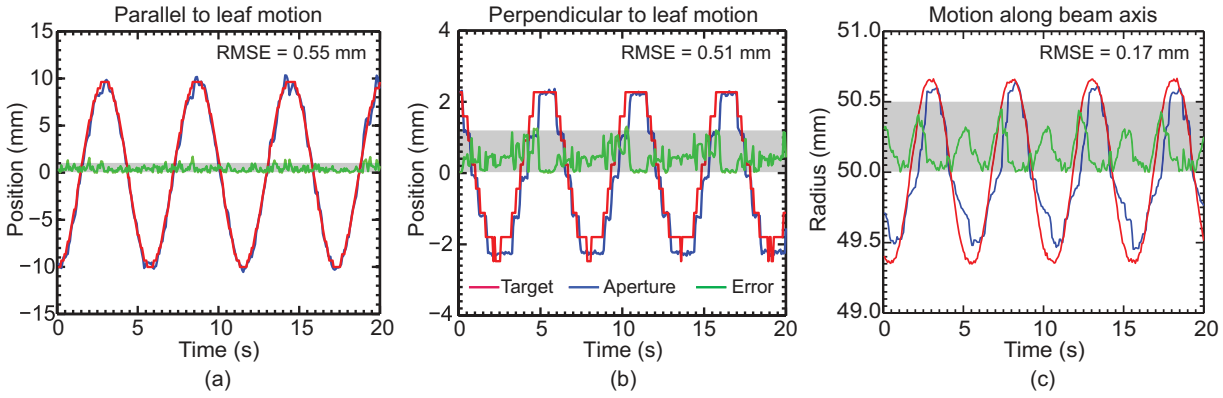

FIG. 8. Geometric accuracy of DMLC tracking (using five subleaves) for target motion (a) parallel and (b) perpendicular to MLC leaf travel, and (c) along the beam axis. The horizontal shaded band denotes an error of 1 mm in (a) and (b) and an error of 0.5 mm in (c).

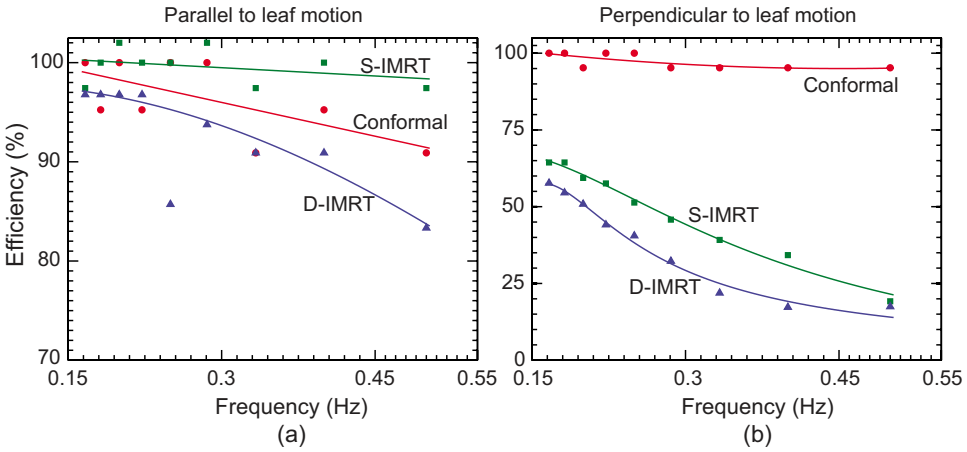

FIG. 9. Tracking efficiency in directions (a) 2 cm parallel and (b) 0.5 cm perpendicular to leaf motion. Results are shown for a conformal (circular) and clinically derived D-IMRT and S-IMRT deliveries. Note the different *y* axes in (a) and (b). Beam holds were not asserted by the MLC controller during the VMAT delivery, and therefore the efficiency was 100%.

direction compared to the parallel direction [Fig. 9(b)]. The IMRT plans used in this study had a few sharp dose gradients in the perpendicular direction, leading to relatively large differences in the "open distances" of some adjacent leaf pairs. As a result, when tracking perpendicular motion, these leaf pairs had to travel a distance that was just within the maximum velocity limit at lower frequencies and well outside this limit at higher frequencies. Finally, it is noteworthy that for target motion parallel to leaf motion [Fig. 9(a)], the efficiency is greater than 80% for all three delivery techniques, even at the highest frequency.

Figure 10 shows the dosimetric impact of DMLC tracking for conformal, D-IMRT, S-IMRT, and VMAT deliveries. In each case, isodose lines at 95%, 70%, 50%, and 20% are shown for delivery to a moving target, in the absence [Figs. 10(a)–10(d)] and presence [Figs. 10(e)–10(h)] of tracking. In addition, the intended dose map is shown in each figure by means of solid lines that correspond to dose delivery to a static target. (Note that, in this early study, the conformal and IMRT deliveries were performed for only one field in each case). In the absence of motion tracking, significant deviations from the intended treatment are observed for all three techniques, with the conformal and S-IMRT deliveries showing relatively large deviations, particularly in the 95% dose regions. The differences are dramatically reduced when tracking is enabled, with all of the isodose curves in each case closely approaching those corresponding to delivery to the static phantom—a result consistent with the submillimeter geometric accuracy observed in Fig. 8. A quantitative measure of the dosimetric impact of DMLC tracking from the data shown in Fig. 10 can be observed from Table I, which lists the results of the gamma index evaluation for all three deliveries in the absence and presence of tracking. Deliveries performed without tracking exhibit between 1.7

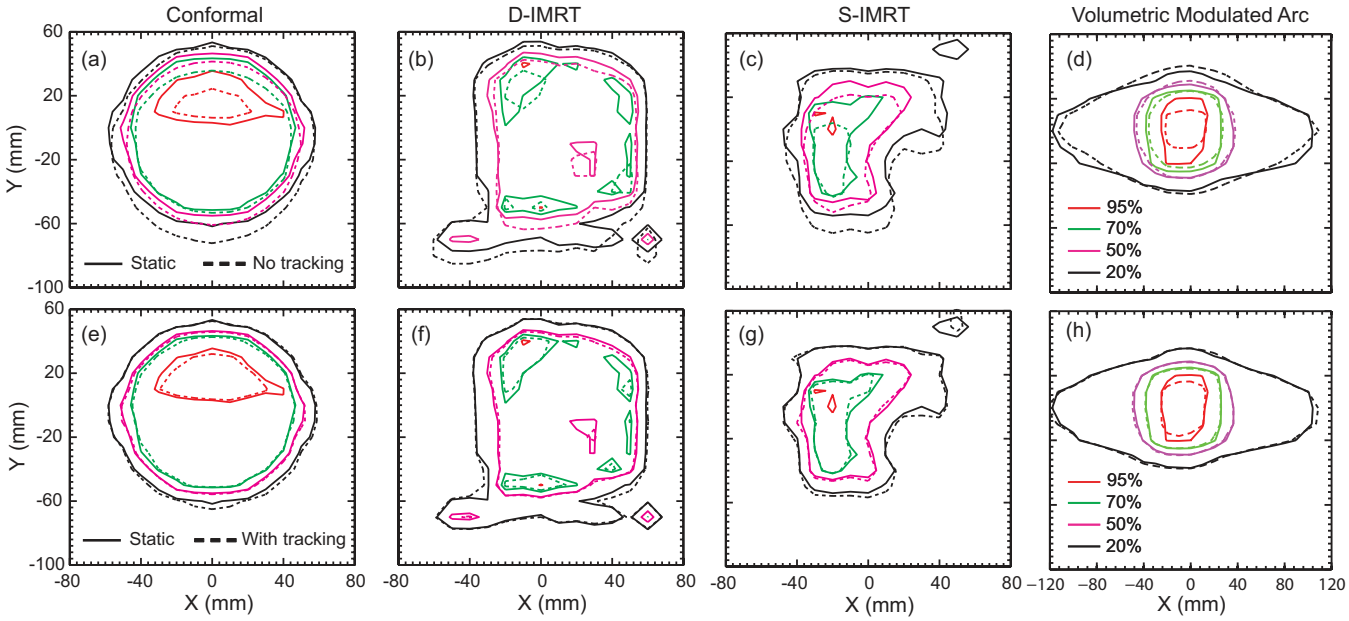

FIG. 10. Isodose (dashed) lines for (a) conformal, (b) D-IMRT (c) S-IMRT, and (d) VMAT deliveries without tracking and corresponding curves [(e), (f), (g), and (h)] with tracking for a target moving 2 cm parallel and 0.5 cm perpendicular to the leaf motion direction. For comparison, isodose curves for delivery to a static object are shown in each figure by solid lines.

TABLE I. Dosimetric error in terms of the percentage of ion-chamber dose values failing a γ index criterion of 3%, 3 mm with respect to delivery to a static phantom from the results shown in Fig. 10. When in motion, the target was moving 20 mm parallel and 5 mm perpendicular to the direction of leaf motion.

	Points failing γ index evaluation (%)	
Delivery	No tracking	With tracking
Conformal	36.0	7.5
S-IMRT	58.8	35.1
D-IMRT	40.3	17.7
VMAT	41.7	11.0

(S-IMRT) and 4.8 (D-IMRT) times more dose points that fail the gamma evaluation compared to corresponding deliveries with DMLC tracking.

V. DISCUSSION

To our knowledge, this is the first empirical demonstration of 3D DMLC-based target tracking. The submillimeter geometric accuracy and the high levels of dosimetric conformality observed in this work are strong indicators of the improvements that DMLC tracking can achieve for the effective management of intrafraction motion. The robustness of the tracking algorithm has been demonstrated by the fact that it was applied without modification to three of the most commonly used delivery techniques (conformal, D-IMRT, and S-IMRT) as well as the evolving VMAT technique. It is also important to note that in addition to the laboratory system, these plans were also delivered using a clinical linac with minimal setup modifications, demonstrating a clear path toward clinical integration.

Nevertheless, before this goal of clinical integration can be realized, a number of issues need to be addressed. For example, new quality assurance protocols will need to be developed for routine DMLC tracking. However, similar procedures exist for other real-time tracking systems such as the Synchrony (Accuray, Sunnyvale, CA) and could be potentially adapted for DMLC-equipped linacs.

Perhaps the most important issue is the need to improve the efficiency of dose delivery. As observed from the results presented in Fig. 9, the delivery efficiency in current DMLC systems drops as the speed of the target increases. The most direct approach to solving this problem is to redesign the MLC with faster leaves. (The currently available DMLCs were never designed with real-time tracking in mind). Another approach would be to develop a DMLC with movable carriages. In such a design, carriage motion would account for most of the target motion along the perpendicular direction and the (much smaller amount of) differential target motion along the perpendicular direction could be resolved through individual leaf motion. Obviously, such modifications would require considerable commitments of time and engineering resources.

An alternate approach, which could be implemented using current MLC technology, is to modify the MLC leaf sequence in order to account for target motion with the least amount of error. Such approaches, which have been described by other groups, can be based on obtaining *a priori* information of target motion, e.g., from a planning 4D CT and/or from an in-room cone-beam 4D CT, and developing a "deliverable" optimized plan (and a corresponding leaf sequence) that accounts for target motion as well as maximum leaf velocities.[35,37] This approach can also be extended to the case where no *a priori* knowledge about target motion is assumed. For each leaf pair, one of the leaves is moved at maximum velocity, while the velocity of the other leaf is dynamically recalculated so as to compensate for instantaneous changes in target position.[35] An additional approach to improve efficiency is to account only for changes in the mean target position with time, rather than tracking individual respiratory cycles.[50,51] This approach trades accuracy for efficiency and may be a viable strategy to account for motion perpendicular to the MLC leaf travel direction where efficiency (Fig. 9) is a concern for motion of the order of 5 mm or more. It should be noted that, while current delivery efficiencies for tracking may be comparable to those for gating, the former approach results in less residual motion, and therefore can potentially achieve significantly more margin reduction.

Another desirable goal for DMLC tracking is to account for more complex forms of target motion. The present algorithm can be extended in a fairly straightforward manner to account for in-plane rotation, which can be treated as an affine transformation. However, accounting for target deformation and/or out-of-plane rotation presents significant challenges. It has been shown that while there is no "exact" solution to this problem, there exist strategies that can be employed in order to dynamically modify MLC leaf positions so as to minimize geometric errors in conforming to deforming targets.[36] The MLC is well-suited to these tasks as each leaf is controlled independently and can be considered a degree of freedom for repositioning and reoptimization.

The ultimate accuracy of any motion compensation strategy, including DMLC tracking, depends on the degree to which real-time information from external and internal surrogates represents the instantaneous state of the target. While internal radio-opaque surrogates can usually provide more reliable information than external markers, the use of the former involves a necessary tradeoff between information quality and increased imaging dose. A possible strategy is to acquire low-dose fluoroscopic images of a region of interest rather than a full field in order to limit the imaging dose. Another attractive possibility is the adaptation of commercially available technologies based on internal electromagnetic markers to yield real-time information.[15]

Finally, the fact remains that the current algorithm is based on a purely geometric transformation of the beam aperture(s) and represents only a first-order approach as it does not perform higher order corrections for changes in the overlying or underlying anatomy, varying field size, off-axis effects, etc. The ideal radiotherapy tracking system would have complete knowledge of the instantaneous state of the entire irradiated volume and would be able to adapt the fluence by

performing on-the-fly optimization during dose delivery. The future realization of such optimized radiotherapy delivery will likely depend on the successful development and incorporation of novel forms of image guidance such as integrated MRI+linac systems[52–55] as well as ongoing increases in computational speed and parallelization.

VI. CONCLUSION

The 3D real-time DMLC tracking algorithm described and empirically demonstrated in this work represents a viable and attractive solution for intrafraction motion management. The algorithm was demonstrated to be equally applicable to a variety of commonly used radiation delivery techniques. Geometric and dosimetric measurements indicate that submillimeter geometric accuracy and very high dosimetric conformality can be achieved using this methodology. While these initial studies are highly promising, a number of challenges need to be addressed prior to clinical integration of this technique.

ACKNOWLEDGMENTS

This work was supported by funds from the National Institutes of Health, (Grant No. R01 93626) and Varian Medical Systems. The authors are grateful to Dr. Byungchul Cho, Dr. Annie Hsu, and Dr. Per Poulsen, Stanford University, for assistance with the dosimetric measurements and to Dr. Karl Otto, Vancouver Cancer Center, Canada, for contributing the MLC plan used in the volumetric arc experiments. The authors would also like to thank Dr. Michelle Svatos, Varian Medical Systems, for carefully reading the manuscript and providing insightful comments.

[a]Author to whom all correspondence should be addressed. Electronic mail: aswant@stanford.edu

[1]G. Hugo, S. Tenn, and N. Agazaryan, "An evaluation of intrafraction motion-induced error for fractionated IMRT delivery," Med. Phys. **30**, 1470–1470 (2003).
[2]R. George, P. J. Keall, V. R. Kini, S. S. Vedam, J. V. Siebers, Q. Wu, M. H. Lauterbach, D. W. Arthur, and R. Mohan, "Quantifying the effect of intrafraction motion during breast IMRT planning and dose delivery," Med. Phys. **30**, 552–562 (2003).
[3]E. Huang, L. Dong, A. Chandra, D. A. Kuban, I. I. Rosen, A. Evans, and A. Pollack, "Intrafraction prostate motion during IMRT for prostate cancer," Int. J. Radiat. Oncol., Biol., Phys. **53**, 261–268 (2002).
[4]P. J. Keall, G. S. Mageras, J. M. Balter, R. S. Emery, K. M. Forster, S. B. Jiang, J. M. Kapatoes, D. A. Low, M. J. Murphy, B. R. Murray, C. R. Ramsey, M. B. Van Herk, S. S. Vedam, J. W. Wong, and E. Yorke, "The management of respiratory motion in radiation oncology report of AAPM Task Group 76," Med. Phys. **33**, 3874–3900 (2006).
[5]J. Wulf, K. Baier, G. Mueller, and M. P. Flentje, "Dose-response in stereotactic irradiation of lung tumors," Radiother. Oncol. **77**, 83–87 (2005).
[6]R. C. McGarry, L. Papiez, M. Williams, T. Whitford, and R. D. Timmerman, "Stereotactic body radiation therapy of early-stage non-small-cell lung carcinoma: Phase I study," Int. J. Radiat. Oncol., Biol., Phys. **63**, 1010–1015 (2005).
[7]R. Komaki, R. S. Swann, D. S. Ettinger, B. S. Glisson, A. B. Sandler, B. Movsas, J. Suh, and R. W. Byhardt, "Phase I study of thoracic radiation dose escalation with concurrent chemotherapy for patients with limited small-cell lung cancer: Report of Radiation Therapy Oncology Group (RTOG) protocol 97-12," Int. J. Radiat. Oncol., Biol., Phys. **62**, 342–350 (2005).
[8]S. L. S. Kwa, J. V. Lebesque, J. C. M. Theuws, L. B. Marks, M. T. Munley, G. Bentel, D. Oetzel, U. Spahn, R. K. Ten Haken, R. E. Drzymala, J. A. Purdy, A. S. Lichter, M. K. Martel, and R. K. TEN Haken, "Radiation pneumonitis as a function of mean lung dose: An analysis of pooled data of 540 patients," Int. J. Radiat. Oncol., Biol., Phys. **42**, 1–9 (1998).
[9]M. L. Hernando, L. B. Marks, G. C. Bentel, S. M. Zhou, D. Hollis, S. K. Das, M. Fan, M. T. Munley, T. D. Shafman, M. S. Anscher, and P. A. Lind, "Radiation-induced pulmonary toxicity: A dose-volume histogram analysis in 201 patients with lung cancer," Int. J. Radiat. Oncol., Biol., Phys. **51**, 650–659 (2001).
[10]A. Schweikard, G. Glosser, M. Bodduluri, M. J. Murphy, and J. R. Adler, "Robotic motion compensation for respiratory movement during radiosurgery," Comput. Aided Surg. **5**, 263–277 (2000).
[11]H. Shirato, S. Shimizu, T. Kunieda, K. Kitamura, M. van Herk, K. Kagei, T. Nishioka, S. Hashimoto, K. Fujita, H. Aoyama, K. Tsuchiya, K. Kudo, and K. Miyasaka, "Physical aspects of a real-time tumor-tracking system for gated radiotherapy," Int. J. Radiat. Oncol., Biol., Phys. **48**, 1187–1195 (2000).
[12]M. Stock, K. Kontrisova, K. Dieckmann, J. Bogner, R. Poetter, and D. Georg, "Development and application of a real-time monitoring and feedback system for deep inspiration breath hold based on external marker tracking," Med. Phys. **33**, 2868–2877 (2006).
[13]X. Tang, G. C. Sharp, and S. B. Jiang, "Fluoroscopic tracking of multiple implanted fiducial markers using multiple object tracking," Phys. Med. Biol. **52**, 4081–4098 (2007).
[14]H. Yan, F. F. Yin, G. P. Zhu, M. Ajlouni, and J. H. Kim, "The correlation evaluation of a tumor tracking system using multiple external markers," Med. Phys. **33**, 4073–4084 (2006).
[15]T. R. Willoughby, P. A. Kupelian, J. Pouliot, K. Shinohara, M. Aubin, M. Roach, III, L. L. Skrumeda, J. M. Balter, D. W. Litzenberg, S. W. Hadley, J. T. Wei, and H. M. Sandler, "Target localization and real-time tracking using the Calypso 4D localization system in patients with localized prostate cancer," Int. J. Radiat. Oncol., Biol., Phys. **65**, 528–534 (2006).
[16]D. Litzenberg, L. A. Dawson, H. Sandler, M. G. Sanda, D. L. McShan, R. K. Ten Haken, K. L. Lam, K. K. Brock, and J. M. Balter, "Daily prostate targeting using implanted radiopaque markers," Int. J. Radiat. Oncol., Biol., Phys. **52**, 699–703 (2002).
[17]T. Xu, J. T. Wong, P. M. Shikhaliev, J. L. Ducote, M. S. Al-Ghazi, and S. Molloi, "Real-time tumor tracking using implanted positron emission markers: concept and simulation study," Med. Phys. **33**, 2598–2609 (2006).
[18]J. S. Kuo, C. Yu, Z. Petrovich, and M. L. Apuzzo, "The CyberKnife stereotactic radiosurgery system: Description installation and an initial evaluation of use and functionality," Neurosurgery **53**, 1235–1239 (2003).
[19]D. W. Andrews, G. Bednarz, J. J. Evans, and B. Downes, "A review of three current radiosurgery systems," Surg. Neurol. **66**, 559–564 (2006).
[20]Y. Kamino, K. Takayama, M. Kokubo, Y. Narita, E. Hirai, N. Kawawda, T. Mizowaki, Y. Nagata, T. Nishidai, and M. Hiraoka, "Development of a four-dimensional image-guided radiotherapy system with a gimbaled X-ray head," Int. J. Radiat. Oncol., Biol., Phys. **66**, 271–278 (2006).
[21]W. D. D' Souza, S. A. Naqvi, and C. X. Yu, "Real-time intra-fraction-motion tracking using the treatment couch: A feasibility study," Phys. Med. Biol. **50**, 4021–4033 (2005).
[22]E. C. Ford, G. S. Mageras, E. Yorke, K. E. Rosenzweig, R. Wagman, and C. C. Ling, "Evaluation of respiratory movement during gated radiotherapy using film and electronic portal imaging," Int. J. Radiat. Oncol., Biol., Phys. **52**, 522–531 (2002).
[23]R. Wagman, E. Yorke, E. Ford, P. Giraud, G. Mageras, B. Minsky, and K. Rosenzweig, "Respiratory gating for liver tumors: Use in dose escalation," Int. J. Radiat. Oncol., Biol., Phys. **55**, 659–668 (2003).
[24]P. Keall, S. Vedam, R. George, C. Bartee, J. Siebers, F. Lerma, E. Weiss, and T. Chung, "The clinical implementation of respiratory-gated intensity-modulated radiotherapy," Med. Dosim. **31**, 152–162 (2006).
[25]Z. Wang, C. G. Willett, and F. F. Yin, "Reduction of organ motion by combined cardiac gating and respiratory gating," Int. J. Radiat. Oncol., Biol., Phys. **68**, 259–266 (2007).
[26]R. S. Ahmed, S. Shen, R. Ove, J. Duan, J. B. Fiveash, and S. M. Russo, "Intensity modulation with respiratory gating for radiotherapy of the pleural space," Med. Dosim. **32**, 16–22 (2007).
[27]R. E. Wurm, F. Gum, S. Erbel, L. Schlenger, D. Scheffler, D. Agaoglu, R. Schild, B. Gebauer, P. Rogalla, M. Plotkin, K. Ocran, and V. Budach, "Image guided respiratory gated hypofractionated Stereotactic Body Radiation Therapy (H-SBRT) for liver and lung tumors: Initial experience," Acta Oncol. **45**, 881–889 (2006).
[28]R. W. Underberg, J. R. van Sornsen de Koste, F. J. Lagerwaard, A. Vin-

cent, B. J. Slotman, and S. Senan, "A dosimetric analysis of respiration-gated radiotherapy in patients with stage III lung cancer," Radiat. Oncol. **1** (2006), published online 2006 March 31, doi: 10.1186/1748-717X-1-8.
[29]J. W. Wong, M. B. Sharpe, D. A. Jaffray, V. R. Kini, J. M. Robertson, J. S. Stromberg, and A. A. Martinez, "The use of active breathing control (ABC) to reduce margin for breathing motion," Int. J. Radiat. Oncol., Biol., Phys. **44**, 911–919 (1999).
[30]D. Mah, J. Hanley, K. E. Rosenzweig, E. Yorke, L. Braban, C. C. Ling, S. A. Leibel, and G. Mageras, "Technical aspects of the deep inspiration breath-hold technique in the treatment of thoracic cancer," Int. J. Radiat. Oncol., Biol., Phys. **48**, 1175–1185 (2000).
[31]K. E. Rosenzweig, J. Hanley, D. Mah, G. Mageras, M. Hunt, S. Toner, C. Burman, C. C. Ling, B. Mychalczak, Z. Fuks, and S. A. Leibel, "The deep inspiration breath-hold technique in the treatment of in operable non-small-cell lung cancer," Int. J. Radiat. Oncol., Biol., Phys. **48**, 81–87 (2000).
[32]Y. Negoro, Y. Nagata, T. Aoki, T. Mizowaki, N. Araki, K. Takayama, M. Kokubo, S. Yano, S. Koga, K. Sasai, Y. Shibamoto, and M. Hiraoka, "The effectiveness of an immobilization device in conformal radiotherapy for lung tumor: Reduction of respiratory tumor movement and evaluation of the daily setup accuracy," Int. J. Radiat. Oncol., Biol., Phys. **50**, 889–898 (2001).
[33]I. Lax, H. Blomgren, I. Naslund, and R. Svanstrom, "Stereotactic radiotherapy of malignancies in the abdomen. Methodological aspects," Acta Oncol. **33**, 677–683 (1994).
[34]L. Papiez, D. Rangaraj, and P. Keall, "Real-time DMLC IMRT delivery for mobile and deforming targets," Med. Phys. **32**, 3037–3048 (2005).
[35]R. McMahon, L. Papiez, and D. Rangaraj, "Dynamic-MLC leaf control utilizing on-flight intensity calculations: A robust method for real-time IMRT delivery over moving rigid targets," Med. Phys. **34**, 3211–3223 (2007).
[36]J. R. McClelland, S. Webb, D. McQuaid, D. M. Binnie, and D. J. Hawkes, "Tracking 'differential organ motion' with a 'breathing' multileaf collimator: Magnitude of problem assessed using 4D CT data and a motion-compensation strategy," Phys. Med. Biol. **52**, 4805–4826 (2007).
[37]D. McQuaid and S. Webb, "IMRT delivery to a moving target by dynamic MLC tracking: Delivery for targets moving in two dimensions in the beam's eye view," Phys. Med. Biol. **51**, 4819–4839 (2006).
[38]P. J. Keall, H. Cattell, D. Pokhrel, S. Dieterich, K. H. Wong, M. J. Murphy, S. S. Vedam, K. Wijesooriya, and R. Mohan, "Geometric accuracy of a real-time target tracking system with dynamic multileaf collimator tracking system," Int. J. Radiat. Oncol., Biol., Phys. **65**, 1579–1584 (2006).
[39]P. J. Keall, A. D. Lauve, M. P. Hagan, and J. V. Siebers, "A strategy to correct for intrafraction target translation in conformal prostate radiotherapy: Simulation results," Med. Phys. **34**, 1944–1951 (2007).
[40]K. Wijesooriya, C. Bartee, J. V. Siebers, S. S. Vedam, and P. J. Keall, "Determination of maximum leaf velocity and acceleration of a dynamic multileaf collimator: Implications for 4D radiotherapy," Med. Phys. **32**, 932–941 (2005).
[41]V. Srivastava, P. J. Keall, A. Sawant, and Y. Suh, "Accurate prediction of intrafraction motion using a modified linear adaptive filter," Med. Phys. **34**, 2546 (2007).
[42]L. E. Court, L. Dong, A. K. Lee, R. Cheung, M. D. Bonnen, J. O'Daniel, H. Wang, R. Mohan, and D. Kuban, "An automatic CT-guided adaptive radiation therapy technique by online modification of multileaf collimator leaf positions for prostate cancer," Int. J. Radiat. Oncol., Biol., Phys. **62**, 154–163 (2005).
[43]Y. Feng, C. Castro-Pareja, R. Shekhar, and C. Yu, "Direct aperture deformation: An interfraction image guidance strategy," Med. Phys. **33**, 4490–4498 (2006).
[44]M. R. Arnfield, J. V. Siebers, J. O. Kim, Q. Wu, P. J. Keall, and R. Mohan, "A method for determining multileaf collimator transmission and scatter for dynamic intensity modulated radiotherapy," Med. Phys. **27**, 2231–2241 (2000).
[45]N. Tyagi, J. M. Moran, D. W. Litzenberg, A. F. Bielajew, B. A. Fraass, and I. J. Chetty, "Experimental verification of a Monte Carlo-based MLC simulation model for IMRT dose calculation," Med. Phys. **34**, 651–663 (2007).
[46]Y. Seppenwoolde, H. Shirato, K. Kitamura, S. Shimizu, M. van Herk, J. V. Lebesque, and K. Miyasaka, "Precise and real-time measurement of 3D tumor motion in lung due to breathing and heartbeat, measured during radiotherapy," Int. J. Radiat. Oncol., Biol., Phys. **53**, 822–834 (2002).
[47]R. George, S. S. Vedam, T. D. Chung, V. Ramakrishnan, and P. J. Keall, "The application of the sinusoidal model to lung cancer patient respiratory motion," Med. Phys. **32**, 2850–2861 (2005).
[48]E. Weiss, K. Wijesooriya, S. V. Dill, and P. J. Keall, "Tumor and normal tissue motion in the thorax during respiration: Analysis of volumetric and positional variations using 4D CT," Int. J. Radiat. Oncol., Biol., Phys. **67**, 296–307 (2007).
[49]K. Otto, "Volumetric modulated arc therapy: IMRT in a single gantry arc," Med. Phys. **35**, 310–317 (2008).
[50]A. Trofimov, C. Vrancic, T. C. Y. Chan, G. C. Sharp, and T. Bortfeld, "Tumor trailing strategy for intensity-modulated radiation therapy of moving targets," Med. Phys. **35**, 1718–1733 (2008).
[51]R. George, J. Williamson, M. Murphy, E. Weiss, and P. Keall, "On the accuracy of a moving average algorithm for tracking respiratory motion during radiation therapy treatment delivery," Med. Phys. **33**, 1986 (2006).
[52]J. J. Lagendijk, B. W. Raaymakers, A. J. Raaijmakers, J. Overweg, K. J. Brown, E. M. Kerkhof, R. W. van der Put, B. Hardemark, M. van Vulpen, and U. A. van der Heide, "MRI/linac integration," Radiother. Oncol. **86**, 25–29 (2008).
[53]J. F. Dempsey, D. Benoit, J. R. Fitzsimmons, A. Haghighat, J. G. Li, D. A. Low, S. Mutic, J. R. Palta, H. E. Romeijn, and G. E. Sjoden, "A device for real-time 3D image-guided IMRT," Int. J. Radiat. Oncol., Biol., Phys. **63**, S202 (2005).
[54]B. Fallone, M. Carlone, B. Murray, S. Rathee, T. Stanescu, S. Steciw, K. Wachowicz, and C. Kirkby, "Development of a linac-MRI system for real-time ART," Med. Phys. **34**, 2547 (2007).
[55]A. J. Raaijmakers, B. W. Raaymakers, and J. J. Lagendijk, "Integrating a MRI scanner with a 6 MV radiotherapy accelerator: Dose increase at tissue-air interfaces in a lateral magnetic field due to returning electrons," Phys. Med. Biol. **50**, 1363–1376 (2005).
[56]See EPAPS Document No. E-MPHYA6-35-054805 for a movie showing real-time DMLC tracking. For more information on EPAPS, see http://aip.org/pubservs/epaps.html.